International Journal of Nanomedicine

Dovepress
Taylor & Francis Group

Open Access Full Text Article

ORIGINAL RESEARCH

Platelet Membrane-Based Nanoparticles for Targeted Delivery of Deferoxamine to Alleviate Brain Injury Induced by Ischemic Stroke

Peina Wang[1,2,*], Xin Lv[1,*], Siyu Tian[1], Wen Yang[2], Mudi Feng[1], Shiyang Chang[2], Linhao You[1], Yan-Zhong Chang[1]

[1]Laboratory of Molecular Iron Metabolism, Key Laboratory of Animal Physiology, Biochemistry and Molecular Biology of Hebei Province, Ministry of Education Key Laboratory of Molecular and Cellular Biology, Department of Physiology, College of Life Science, Hebei Normal University, Shijiazhuang, Hebei Province, 050024, People's Republic of China; [2]Department of Histology and Embryology, College of Basic Medical Sciences, Hebei Medical University, Shijiazhuang, Hebei Province, 050017, People's Republic of China

*These authors contributed equally to this work

Correspondence: Yan-Zhong Chang; Peina Wang, Email chang7676@163.com; 19301641@hebmu.edu.cn

Background: Timely thrombolysis serves as the primary therapeutic approach for ischemic stroke, one of the most serious global public health problems, although reperfusion can cause severe ischemia reperfusion (I/R) injury. Oxidative stress and activation of cell death pathways are the main mechanisms of I/R injury. Our previous studies have demonstrated that iron overload stimulates the generation of reactive oxygen species and facilitates the activation of iron-dependent ferroptosis in the pathogenesis of I/R injury. Removal of excess free iron by deferoxamine (DFO), an iron chelator, may inhibit iron toxicity and reverse I/R-induced neurological deficits. Despite its therapeutic potential, DFO's clinical translation for I/R injury is hampered by rapid systemic clearance, suboptimal bioavailability, and a lack of ischemic lesion-targeting ability. Nanoscale delivery platforms enabling targeted DFO release in stroke lesions may overcome these pharmacokinetic barriers and enhance clinical outcomes.

Methods: On the basis of the properties of liposomes in carrying hydrophilic substances and crossing the leaky blood–brain barrier in cerebral I/R, we first encapsulated DFO within traditional liposomes to improve its biocompatibility. Subsequently, inspired by the natural homing properties of platelets to damaged blood vessels during I/R injury, the isolated platelet membranes were coated onto the DFO-liposomes, thus endowing the nanodrug with the ability to target stroke lesion.

Results: Our results demonstrate that Platesome-DFO exhibits accurate lesion-targeting ability and significantly decreases lesion iron content, thereby preventing neuronal ferroptosis and ultimately reversing neurological deficits in I/R mice.

Conclusion: Platesome-DFO provides a novel therapeutic approach for cerebral I/R injury by regulating brain iron status and iron-dependent pathways, highlighting its promising application in the clinical treatment of cerebral I/R injury.

Keywords: ischemic stroke, iron, ferroptosis, deferoxamine, platelet membrane, nanomedicine

Introduction

Stroke is an acute and severe cerebrovascular disease with high morbidity, mortality, and medical cost. It has been reported that ischemic stroke, which results from a lack of blood supply to the brain, accounts for approximately 84% of all stroke cases.[1] Irreversible neurological injury can be avoided only if the blocked blood vessels are reperfused within the therapeutic time window. However, ischemia/reperfusion (I/R) can immediately cause dysregulation of oxidation and antioxidation, disrupt the balance between the generation and scavenging of reactive oxygen species (ROS), eventually leading to the accumulation of ROS in the ischemic brain, which exacerbates the activation of inflammatory responses and results in secondary neurological damage.[2] Therefore, I/R injury is considered the main culprit and an inevitable obstacle in the therapy of ischemic stroke. Despite the development of various drugs and functional nanoparticles with ROS scavenging ability, effective treatment options for I/R injury remain disappointingly limited.

Received: 8 January 2025
Accepted: 8 June 2025
Published: 16 June 2025

Many studies have indicated that a higher iron status is a critical risk factor associated with neuronal damage following cerebral I/R. Standard clinical analysis has repeatedly shown that elevated plasma ferritin levels are associated with poor outcomes in patients with ischemic stroke.[3,4] Iron overload exacerbates brain edema and hemorrhagic transformation in ischemic stroke patients receiving thrombolytic therapy with tissue plasminogen activator.[5,6] Mechanistically, our previous research has demonstrated that excessive iron exacerbates neuronal damage by catalyzing the Fenton reaction to convert superoxide and hydroxyl radicals into highly reactive toxic radicals or catalyzing lipid peroxidation as a cofactor of lipid oxidation enzymes.[7–9] Of note, we and others have recently described the induction of neuronal ferroptosis, a newly identified form of regulated cell death resulting from the catastrophic accumulation of iron-dependent lipid reactive oxygen species, in I/R brains.[8,10–12] Therefore, iron is a key factor that stimulates ROS generation and facilitates the subsequent activation of cell death pathways, particularly the ferroptosis pathway, in I/R injury. Iron depletion via chelator may protect neuronal cells against ferroptosis and is expected to emerge as a promising strategy for the treatment of cerebral I/R.

Among the clinically available iron chelators, deferoxamine (DFO) has long been used to remove excess iron in iron overload diseases, such as the secondary iron overload that afflicts thalassemia patients, and has been shown to be the most effective option with the most favorable toxicity profile.[13,14] Moreover, DFO has demonstrated its protective effects in animal stroke models of I/R as well as in clinical studies in which ischemic stroke patients administered DFO exhibited improved outcomes.[5,15–17] However, the poor bioavailability and the extremely short plasma half-life (20 min in humans) of DFO limits its use in stroke treatment.[18,19] More important, at the high doses needed to achieve effective concentrations, DFO can cause serious side effects, including renal and liver complications.[13] Another limitation of DFO for use in stroke treatment is that systemic administration does not specifically target to the injured region of the I/R brain. New delivery approaches that can target deliver DFO to the injured brain region and improve the local DFO concentration are expected to provide significant improvements in stroke outcomes.

Despite advancements in stroke-targeted nanoplatforms, such as polymeric carriers, metallic nanoparticles, and carbon-based systems, current materials face persistent translational barriers, including compromised biosafety profiles, suboptimal therapeutic efficacy, and insufficient blood–brain barrier penetrability.[20,21] Recently, cell membrane-based biomimetic cloaking has emerged as a new strategy for enhancing synthetic nanoparticles delivery, leveraging retained membrane functionalities to overcome systemic biological barriers while preserving immunoevasive properties. Platelets (PLT) play a critical role in the development and progression of thrombosis. Previous studies have shown that the platelet membrane exhibits properties in binding to injured vasculature and has advantages for targeting ischemic brain regions.[22–26] Therefore, we propose a new type of PLT membrane-coated biomimetic nanodevice to deliver DFO specifically to the ischemic brain. On the basis of the properties of liposomes in carrying hydrophilic substances and crossing the leaky blood–brain barrier in cerebral I/R,[27] we first encapsulated DFO within traditional liposomes through hydration to improve its biocompatibility. Subsequently, the isolated PLT membranes were coated onto the DFO-liposomes by coextrusion, endowing this nanodrug with stroke lesion targeting ability (Figure 1a). This PLT membrane-cloaked, DFO-loaded nanoliposome, named Platesome-DFO, can deliver DFO to the targeted lesion, increasing intracellular drug concentrations to markedly higher levels than those achievable through systemic administration. Particularly, we confirmed the chelation of excess iron by Plateletsome-DFO, and the consequent inhibition of iron-dependent lipid peroxidation and ferroptosis in the cerebral I/R brain (Figure 1b). 2,3,5-triphenyltetrazolium chloride (TTC) staining measurement from mouse models demonstrated that the Platesome-DFO treatment effectively alleviated I/R-induced brain damage. Our Platesome-DFO formulation offers a viable strategy for specifically targeting lesions to inhibit neuronal death, demonstrating potential to improve outcomes in cerebral I/R injury.

Materials and Methods

Preparation of Platelet Membranes

Platelets were isolated as described previously.[22,28] C57BL/6 mice were anesthetized, and then the whole blood was drawn via cardiac puncture and immediately collected into tubes containing acid citrate dextrose buffer (75×10^{-3} M sodium citrate, 39×10^{-3} M citric acid, 135×10^{-3} M dextrose, pH 7.4). The blood was first centrifuged at 100

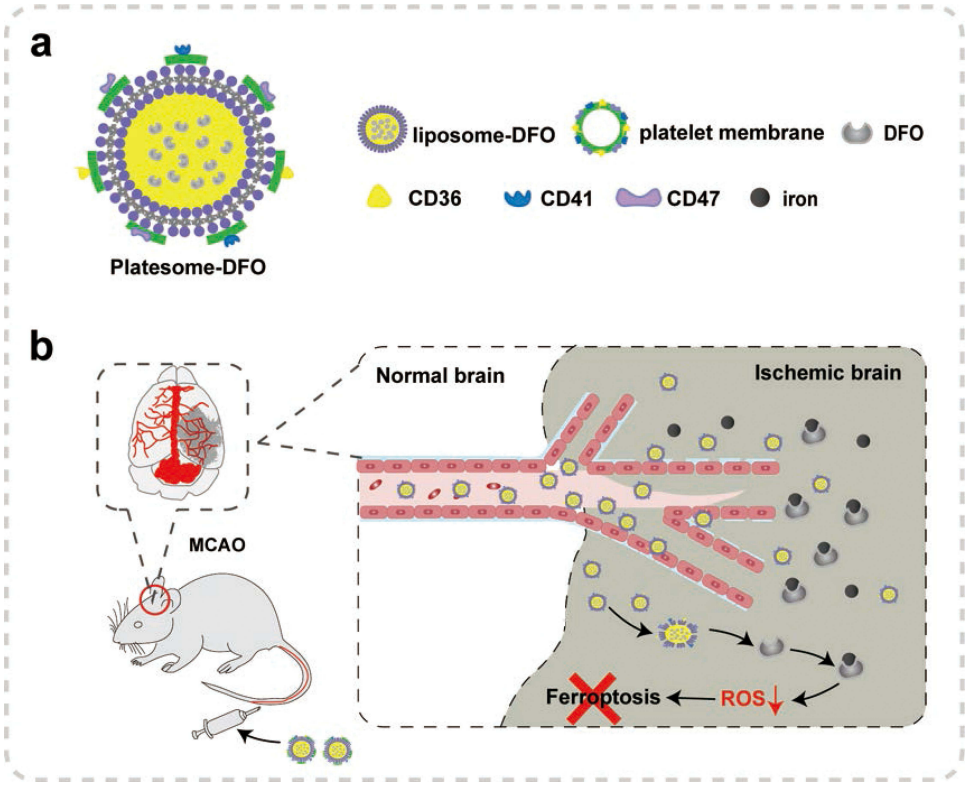

Figure 1 Schematic illustration of Platesome-DFO structure and its proposed protective mechanism in ischemic stroke. (**a**) The Platesome-DFO was fabricated by coextrusion of platelet membranes and Liposome-DFO to form nanoparticles that inherit the natural characteristics of the platelet membrane, including targeting damaged blood vessels and immune escape capabilities, by the presence of specific membrane proteins, such as CD36, CD41, and CD47. (**b**) After intravenous injection, Platesome-DFO is delivered to the injured brain region after stroke, followed by the release of DFO, which chelates excessive iron and inhibits ferroptosis of neuronal cells.

×*g* for 20 min at room temperature, and the platelet-rich supernatant was transferred into another tube and centrifuged at 800 ×*g* for 20 min. The supernatant was discarded, and a red blood cell lysis buffer (Solarbio, China) was added to remove the remaining erythrocytes at 4°C. After 5 min, the solution was centrifuged for 20 min at 800 ×*g* and the platelets were resuspended in modified Tyrode's buffer (134×10^{-3} M NaCl, 2.9×10^{-3} M KCl, 1×10^{-3} M $MgCl_2$, 12×10^{-3} M $NaHCO_3$, 0.34×10^{-3} M Na_2HPO_4, 1×10^{-2} M HEPES, 2×10^{-6} M prostaglandin E1, pH 7.4). The platelet membranes were obtained by a repeated freeze-thaw process. Briefly, the platelet solution was frozen at −80°C for 10 min and then thawed at 25°C. After three freeze-thaw cycles, the platelet membrane vesicles were collected by centrifugation (12,000 ×*g*, 30 min, 4°C) and resuspended in phosphate buffered saline (PBS).

Preparation of PNV, Liposome-DFO, and Platesome-DFO

To fabricate PNV, the purified platelet membrane solution was sonicated for 10 min using a Fisher Scientific FS30D bath sonicator at frequency of 42 kHz and power of 100 W. DFO-loaded liposomes were prepared by thin-film hydration. Briefly, a mixture consisting of lecithin, cholesterol, and 1,2-distearoyl-sn-glycero-3-phosphoethanolamine-N-[methoxy (polyethylene glycol)-2000] (DSPE-mPEG) at a molar ratio of 3.8:2:1 was dissolved in 4 mL alcohol and then transferred into a round-bottom flask. After the alcohol was dried using a vacuum rotary evaporator, a thin film was formed at the bottom of the flask. Next, the film was hydrated with 1 mL PBS containing 50 mg DFO to form a liposome suspension. The resulting liposome suspension was centrifuged using a 30 kDa ultrafiltration device to remove any unencapsulated DFO, followed by extrusion through a liposome extruder with different pore size filters to obtain Liposome-DFO nanoparticles. The preparation of Platesome-DFO was performed by coextruding Liposome-DFO (1 mL) and platelet membranes (1.5×10^9 platelets in 1 mL PBS).

https://doi.org/10.2147/IJN.S516316

Determination of Drug Loading and Encapsulation Efficiency

To measure the content of DFO in the nanoparticles, Liposome-DFO, or Platesome-DFO was solubilized in 0.5% TritonX-100 in HAc-NaAc buffer (pH 6.5) for 2 h to break down the membranes and release DFO. Next, 1 mM ferrous ammonium sulfate hexahydrate ($H_8FeN_2O_8S_2 \cdot 6H_2O$) was added to the solution, and the absorbance of the resulting DFO-Fe compound was measured at 425 nm with a UV spectrometer (U3010, HITACHI, Japan). The DFO loading efficiency and encapsulation efficiency were calculated as follows:

$$\text{Loading efficiency (\%)} = \text{mass of DFO in nanoparticles/total mass of nanoparticles} \times 100\%,$$
$$\text{Encapsulation efficiency (\%)} = \text{mass of DFO in nanoparticles/total mass of DFO} \times 100\%$$

Characterization of Nanoparticles

The morphological characterization of nanoparticles was carried out by TEM, as previously described.[28] In brief, 10 mL samples were dropped onto carbon-coated copper grids. After 5 min of deposition, the residual fluid was removed using filter paper, and then 20 mL 2% uranyl acetate solution was added onto the grids for another 5 min. The images were obtained using a JEM 100SX transmission electron microscope (HITACHI, Japan). The polydispersity index, diameter and zeta potentials of the nanoparticles were measured using a Zeta Sizer Nano series Nano-ZS (Malvern Instruments Ltd, Malvern, UK).

Western Blot Analysis

Protein expression was estimated by Western blot analysis as previously reported.[29] The protein bands were separated by SDS-PAGE and transferred onto an NC membrane. After blocking with 5% milk for 1.5 h at room temperature, the blots were incubated with different primary antibodies overnight at 4°C, followed by incubation with secondary antibodies for 1 h at room temperature. The antibodies used in the study were as follows: anti-β-actin (1:10,000) was obtained from Sigma-Aldrich (#A5441, St Louis, MO, USA); anti-FtH (1:10,000), anti-FtL (1:10,000) anti-ACSL4 (1:5000), anti-GPX4 (1:10,000), anti-CD36 (1:5000), anti-CD41 (1:3000), and anti-CD47 (1:5000) were obtained from Abcam, USA. (#ab183781, #ab109373, #ab155282, #ab125066, #ab252923, #ab181582, #ab218810). The enhanced chemiluminescence (ECL) method was used to detect the immunoreactive proteins. The expression of these proteins was quantified by transmittance densitometry using ImageJ software.

Release Profile of Liposome-DFO and Platesome-DFO

The release of DFO from Liposome-DFO and Platesome-DFO under mimicked physiological conditions was evaluated by dialysis under two different pH values (5 and 7.4), at 37°C. Briefly, 1 mL Liposome-DFO or Platesome-DFO was added to a dialysis bag with a molecular weight cutoff of 18 kDa. The solution was then dialyzed against 10 mL PBS (pH 5 or 7.4) under 100 rpm stirring. The PBS was collected at different time points, followed by incubation with $H_8FeN_2O_8S_2 \cdot 6H_2O$, as described above. Finally, the absorbance of the resulting DFO-Fe compound was determined at 425 nm.

Cell Line

Neuro-2a (N2a) cell line was used in this study. The cells were cultured in Dulbecco's Modified Eagle Medium (DMEM) supplemented with 10% (v/v) heat-inactivated foetal calf serum (FBS), 4.5 mg/mL glucose, 100 μg/mL streptomycin, and 100 U/mL penicillin in a 37°C humidified incubator with 5% CO_2. For cell uptake analysis, the cells were incubated with medium containing free DiO, Liposome-DiO, or Platesome-DiO (20 μM DiO) for 6 h, followed by washing with PBS and resuspension in 1 mL of PBS. The cellular DiO fluorescence intensity was analyzed by flow cytometry (CytoFLEX, Bechman Coulter).

Oxygen and Glucose Deprivation and Reoxygenation

N2a cells were washed twice with deoxygenated, glucose-free DMEM and then maintained in the same medium. After that, the cells were incubated in a hypoxic chamber (1% O_2, 5% CO_2, 94% N_2) at 37°C for 4 h to induce oxygen-glucose deprivation (OGD). Reoxygenation was initiated by replacing the medium with glucose-containing complete DMEM, followed by a 24-hour incubation under normoxic conditions.

Intracellular ROS Detection

The cells were seeded in 6-well dishes and subjected to OGD treatment. During reoxygenation, free DFO, Liposome-DFO, or Platesome-DFO (5 μM DFO) was added. After 24 h of incubation, the cells were harvested by trypsinization and washed with PBS. The cells were resuspended in 500 μL of PBS containing 10 μM 2',7'-Dichlorodihydrofluorescein diacetate (DCFH-DA, S0033, Beyotime, Shanghai, China) and incubated at 37°C for 30 min. After the cells were washed three times with PBS, the fluorescence intensity was measured using a flow cytometer.

Animals

Three-month-old male C57BL/6 mice were maintained in cages at 21°C ± 2°C with controlled humidity (40%) and under a 12 h/12 h light/dark cycle. All animals were provided free access to water and food. All animal procedures conformed to the Guide for the Care and Use of Laboratory Animals published by the US National Institutes of Health (NIH Publication, 8th Edition, 2011), and were approved by the Institutional Animal Care and Use Committee of Hebei Medical University.

Animal Groups and Transient Ischemic Stroke Mouse Model

Transient middle cerebral artery occlusion (60 min) and reperfusion (24 h) surgery was performed to induce ischemic stroke in mice as previously described.[8] In brief, after being anaesthetized, the mice were placed on a heating blanket, and the neck area was exposed. The internal carotid artery (ICA), external carotid artery (ECA), and common carotid artery (CCA) of the mice were isolated. After ligation of the distal ECA, a nylon monofilament (602234PK10Re, Doccol Corp., CA) was inserted from the ECA to the ICA. Sixty minutes later, the suture was removed to commence reperfusion. For the sham operation group, the mice underwent the same procedure as the MCAO group, except for the arterial occlusion. For therapeutic studies, the mice were randomly divided into five groups. Saline, DFO, Liposome-DFO, PNV, or Platesome-DFO (DFO 25 mg/kg) were injected intravenously at the beginning of reperfusion. The mice were sacrificed for further analysis 24 h after injection.

Assessment of Neurologic Deficits

At 24 h after reperfusion, signs of neurologic impairment were evaluated according to a five-point scale: 0, normal; 1, failed to extend right forepaw; 2, circle to the right; 3, fell to the right; 4, could not walk spontaneously; 5, dead.[30]

Assessment of Brain Infarction

After 24 h of reperfusion, the mice were deeply anesthetized, and their brains were immediately removed. To measure the infarction volume, the brains were sliced into 1 mm coronal sections with a metallic brain matrix and then incubated in 2% TTC solution at 37°C for 10 min. The slices were then transferred to 8% paraformaldehyde and stored at 4°C before analysis. The percentage of infarct volume was calculated by the following formula: (contralateral hemisphere volume - non-infarcted ipsilateral hemisphere volume)/contralateral hemisphere volume × 100%.

Quantitative Real-Time PCR Analysis

Total RNA was extracted from the samples using TRIzol reagent according to the manufacturer's instructions. Total RNA (1 mg) was reverse transcribed into cDNA for quantitative real-time PCR. SYBR Green PCR Master Mix (#A301-01, GenStar, Beijing, China) and the Bio-Rad CFX Connect Real-Time System were used. The primer sequences used were the following: Actb: forward: AGGCCCAGAGCAAGAGAGGTA, reverse: TCTCCATGTCGTCCCAGTTG; TNFα:

forward: CCTGTAGCCCACGTCGTAG, reverse: GGGAGTAGACAAGGTACAACCC; IL1β: forward: GAAATGCCACCTTTTGACAGTG, reverse: TGGATGCTCTCATCAGGACAG; IL6: forward: GCTACCAAACTGGATATAATCAGGA, reverse: CCAGGTAGCTATGGTACTCCAGAA, ptgs2: forward: CTGCGCCTTTTCAAGGATGG, reverse: GGGGATACACCTCTCCACCA.

In vivo Biodistribution Study of Nanoparticles

To determine the distribution of nanoparticles in the brain, the stroke mice were randomly divided into three groups and then saline, DiR-labeled Liposome-DFO, or DiR-labeled Platesome-DFO were intravenously administered at the beginning of reperfusion. After 24 h, the brain, heart, liver, spleen, lung, and kidneys of the mice were immediately removed, and the DiR signal was analyzed using a Maestro in vivo imaging system.

Assessment of Malondialdehyde

The MDA content in the different groups was measured using a commercial kit from Beyotime Institute of Biotechnology according to the manufacturer's instructions.[8] The brain tissue was homogenized in 1:9 (w/v) ice-cold saline, and then the homogenate was centrifuged at 10000 ×*g* for 10 min. The supernatant was collected to detect the MDA level at a wavelength of 532 nm by microplate reader.

Measurement of Brain Iron Content

The iron contents of brain samples were determined using ICP-MS as described previously.[8,14] In brief, brain samples were dried at 105°C for 8 h and then resuspended in 1 mL 65% nitric acid overnight at room temperature. The samples were heated for 20 min at 90°C, and then 1 mL 30% H_2O_2 was added at 70°C (20 min) for further digestion. Finally, the samples were diluted in 2 mL ultrapure water and subjected to iron concentration determination by ICP-MS. The concentrations were determined from a standard curve and normalized to the dry tissue weight.

Hemolysis and Blood Coagulation Assays

Whole blood from C57BL/6 mice was collected and then centrifuged at 3000 ×*g* for 10 min to obtain red blood cells. The red blood cells were washed three times with saline and resuspended in saline to a concentration of 1×10^9 cells/mL. Next, the red blood cells were incubated with saline, DFO, Liposome-DFO, PNV, Platesome-DFO, or 0.5% TritonX-100 for 2 h. The solutions were centrifuged at 3000 ×*g* for 10 min and then photographed. The supernatant was collected, and the degree of hemolysis was analyzed by measuring the absorbance at 540 nm. Blood coagulation indices of mice were detected using a prothrombin time assay liquid kit, a thrombin time assay liquid kit, and an activated partial thrombin time liquid kit according to the manufacturer's instruction (Sunbiote, Shanghai, China).

H&E Staining

To evaluate the safety of the nanoparticles, the stroke mice, which were treated with saline, DFO, Liposome-DFO, or Platesome-DFO, were sacrificed and the brain, heart, liver, spleen, lung, and kidney were excised for H&E staining. The samples were fixed in 4% paraformaldehyde at 4°C for 24 h. After being embedded in paraffin, serial 4 mm sections were obtained and then dewaxed in xylene and rehydrated in an ethanol gradient. Finally, the sections were stained with hematoxylin and eosin for microscopic examination.

Statistical Analysis

The data are shown as the mean ± SEM. Statistical analysis was performed with SPSS 16.0 software. Student's *t*-test or one-way ANOVA followed by Tukey's post hoc test was used for comparison between two groups or among multiple groups, respectively. The n value was presented in the figure legends, and differences were considered statistically significant when the *p*-value was < 0.05.

Results

Characterization of Platelet Membrane-Cloaked Deferoxamine-Loaded Nanoliposomes

As shown in Figure 2a, the DFO was first loaded into the liposome vehicle to form Liposome-DFO, after which the Liposome-DFO nanoparticles were enrobed within the platelet membranes, which accrued and purified from mice platelet, using coextrusion method to finally form Platesome-DFO. Transmission electronic microscopy (TEM) images demonstrate that both the Liposome-DFO and Platesome-DFO nanoparticles were spherical structures with diameters of nearly 150 nm (Figure 2b). Dynamic light scattering (DLS) was used to characterize the size, polydispersity, and surface charge of the nanoparticles. As shown in Figure 2c, compared to the platelet membrane nanovesicles (PNV; 203.5 ± 4.5 nm) and the Liposome-DFO (166.9 ± 2.0 nm), the average hydrodynamic diameter of Platesome-DFO was reduced to 136.6 ± 1.6 nm after coextrusion. In addition, the Platesome-DFO also showed a low polydispersity index (PDI), indicating a uniformity in size (Figure 2d). In addition, the zeta potential analysis indicates that the surface charge of Liposome-DFO was approximately −10 mV, while the PNV and Platesome-DFO showed similar surface potentials of about −20 mV, demonstrating successful cloaking of the Platesome-DFO with platelet membrane after coextrusion (Figure 2e). To further evaluate the physicochemical properties and storage stability of Platesome-DFO, we examined the in vitro stability of the formulation in saline. As shown in Figure 2f and g, the Platesome-DFO maintained satisfactory stability in saline at 4°C, with no significant change in its hydrodynamic diameter or PDI after 7 days. We next investigated the DFO release profiles in Phosphate buffered saline (PBS) at pH 5 or 7.4 from both Liposome-DFO and Platesome-DFO; the two nanoparticles showed similar drug release behavior (Figure 2h). About 45% encapsulated DFO was released within 24 h under physiological conditions (pH 7.4), whereas at acid conditions (pH 5.0), about 70% cumulative DFO release was achieved in 24 h, revealing the pH-dependence of DFO release and suggesting that the nanoparticles may discharge their cargo in lysosomes after uptake by neuronal cells.

The targeting of the stroke brain by platelets is mainly regulated by platelet membrane proteins.[22,23,26,31] To further determine whether the Platesome-DFO exhibits a similar membrane protein molecules content as platelets, we examined the presence of three major surface proteins in Platesome-DFO, including adhesion-associated protein CD41, transmembrane glycoprotein CD36, and immunomodulatory protein CD47, by Western blot analysis. Figure 2i and j show the quantification of proteins in platelets (PLT), PNV, Platesome-DFO, and Liposome-DFO, verifying the presence of the platelet-associated surface proteins CD36, CD41, and CD47 on the Platesome-DFO. In addition, Fourier transform infrared (FT-IR) analysis also demonstrated that the protein components of PNV were incorporated into the Platesome-DFO. Compared with Liposome-DFO, one vibration peak between 1655 cm^{-1} to 1542 cm^{-1} can be seen in the spectrum from Platesome-DFO, which is attributed to the cloak of platelet membranes (Figure 2k). These data indicate that we successfully transferred platelet proteins to the Platesome-DFO.

Stroke Lesion Targetability and Biodistribution of Platesome-DFO in vivo

To address whether the nanoparticles can target the injured brain in ischemic stroke, we established a middle cerebral artery occlusion (MCAO) mouse model to mimic cerebral I/R and examined the organismal biodistribution of Liposome-DFO and Platesome-DFO. To this end, we loaded the lipid dye, DiR (1,1'-dioctadecyl-3,3,3',3'-tetramethylindotricarbocyanine iodide), into the liposomes and platesomes to label the nanovesicles. As shown in Figure 3a, the fluorescence signals from the dye molecules in Liposome-DiR and Platesome-DiR were nearly equivalent; the encapsulation efficiencies of Liposome-DiR and Platesome-DiR were 27.4% and 28.4%, respectively (Figure 3b). The mean hydrodynamic diameters of Liposome-DiR and Platesome-DiR were 165.80 ± 0.95 nm and 131.63 ± 0.96 nm, respectively, while the PDI of the two nanoparticles were both around 0.1 (Figure 3c and d). Thus, the characteristics of Liposome-DiR and Platesome-DiR were similar to the nanovesicles loaded with DFO.

Next, we performed MCAO operation on mice and the focal blood flow was measured by laser Doppler flowmetry to confirm the I/R model was successfully established (Figure 3e). At the onset of reperfusion, we intravenously administered nanoparticles to the mice. After 24 h, the mouse brain, and the major organs including heart, lung, liver, spleen, and

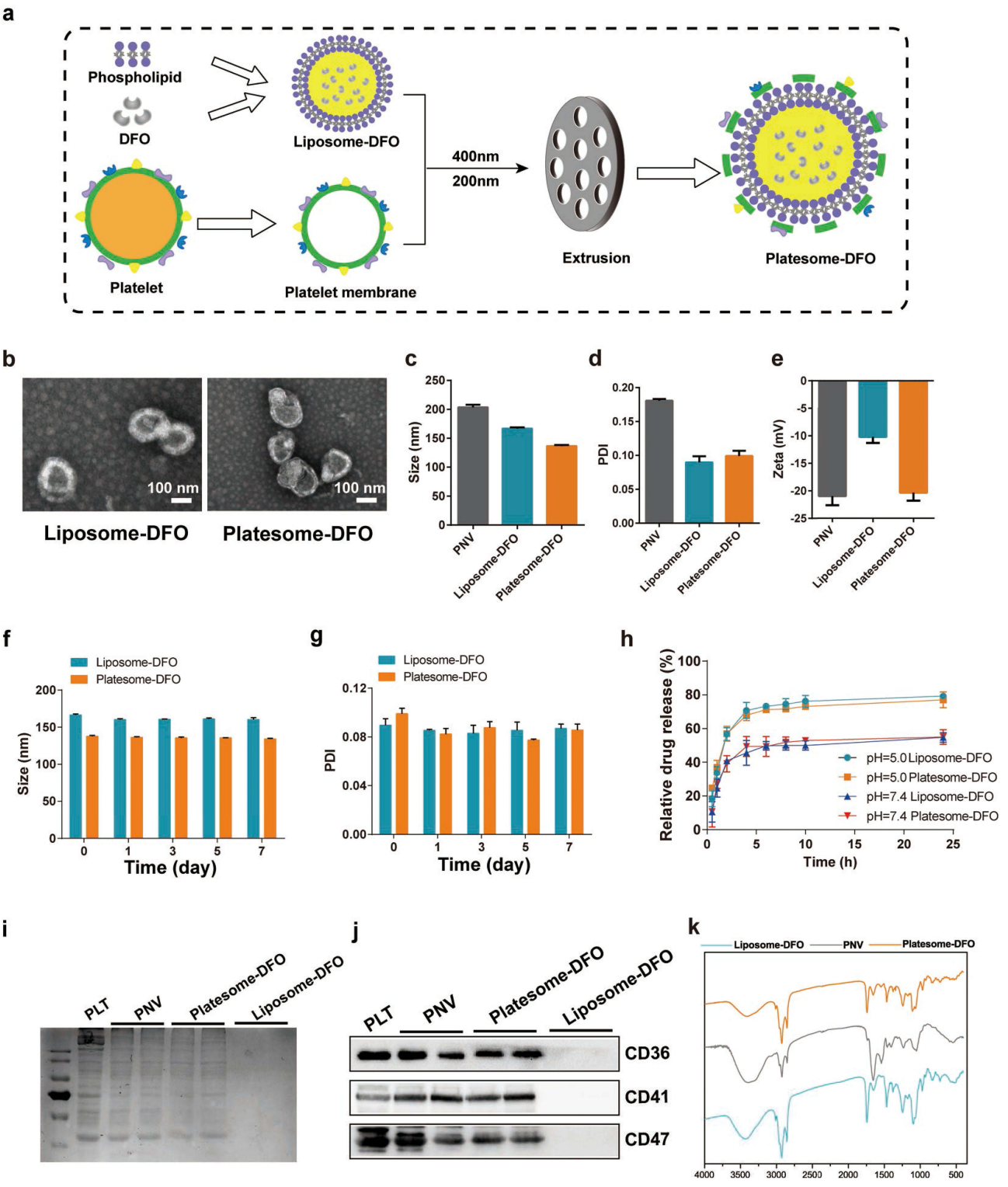

Figure 2 Characterization of platelet membrane-cloaked deferoxamine-loaded liposomes. (**a**) Schematic diagram of the generation of Platesome-DFO by the coextrusion method. (**b**) Transmission electronic microscopy image of Liposome-DFO (left) and Platesome-DFO (right). Scale bar: 100 nm. (**c**) Hydrodynamic diameter, (**d**) PDI and (**e**) surface zeta potential of PNV, Liposome-DFO and Platesome-DFO. (**f**) Hydrodynamic diameter and (**g**) PDI of Liposome-DFO and Platesome-DFO in saline after incubation for the indicated time intervals as determined by DLS. (**h**) DFO release characteristics of Liposome-DFO and Platesome-DFO under physiological conditions (pH 7.4) and acidic conditions (pH 5.0) over 24 h. (**i**) SDS-PAGE analysis of total proteins isolated from PLT, PNV, Platesome-DFO, and Liposome-DFO. (**j**) Western blot analysis of platelet membrane proteins, including CD36, CD41, and CD47, in platelets, PNV, Platesome-DFO, and Liposome DFO. (**k**) FT-IR spectra of Liposome-DFO, PNV, and Platesome-DFO. Data are expressed as mean ± SEM. Data are expressed as mean ± SEM. (n = 3).

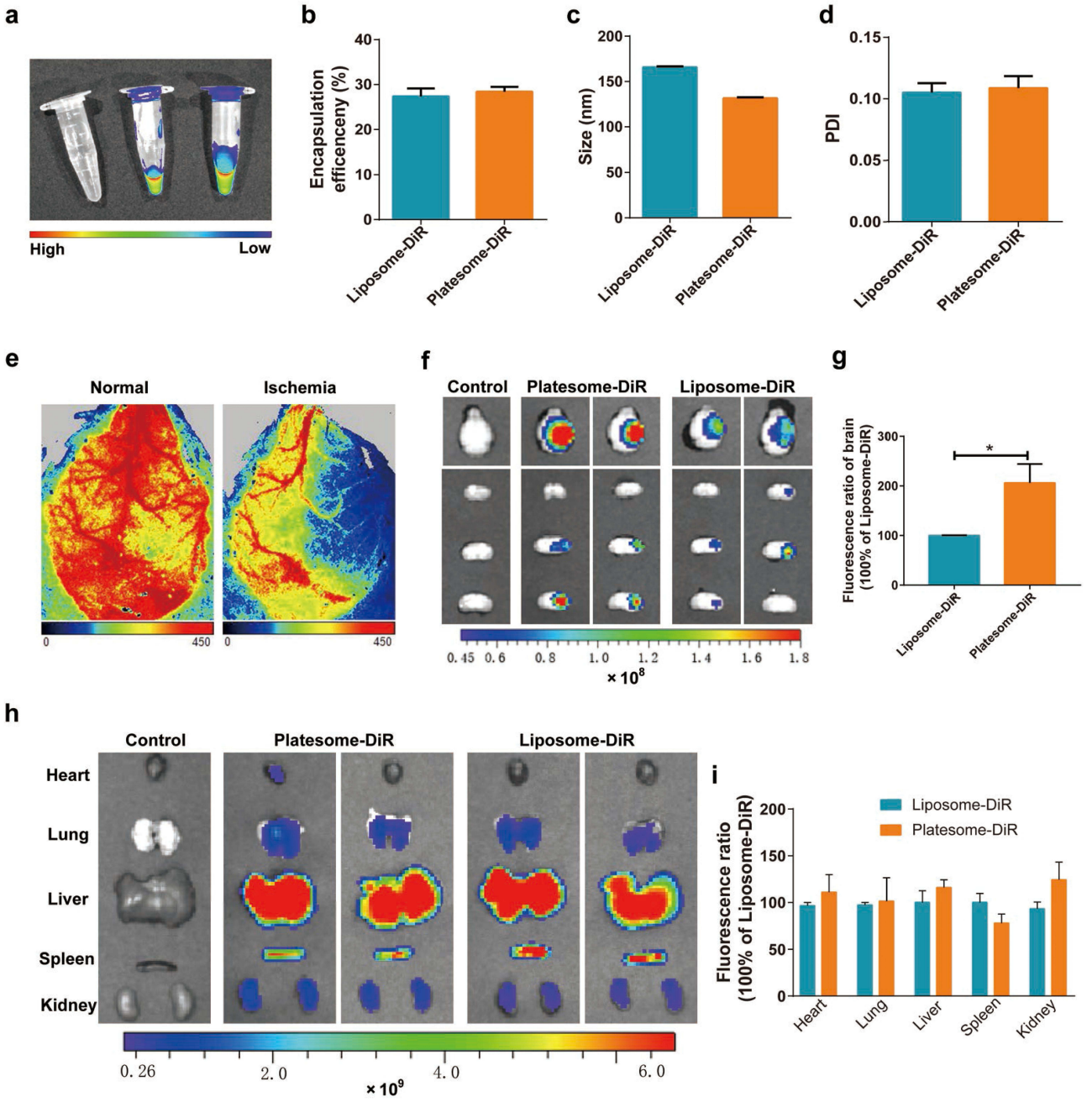

Figure 3 Stroke lesion targetability and biodistribution of Platesome-DFO in vivo. (**a**) DiR fluorescence images of control (left), Liposome-DiR (middle), and Platesome-DiR (right) formulations. (**b**) Encapsulation efficiencies of DiR in Liposome-DiR and Platesome-DiR, as measured by spectrophotometry. (**c**) Hydrodynamic diameter and (**d**) PDI of Liposome-DiR and Platesome-DiR. (**e**) The cerebral ischemia reperfusion model was induced by MCAO for 60 min with a subsequent 24 h reperfusion. Blood flow was measured by laser Doppler flowmetry during MCAO. (**f**) Ex vivo fluorescence images of DiR-labeled Liposome-DFO and Platesome-DFO in the ischemic brain and brain sections at 24 h. (**g**) Fluorescence ratio of the ischemic hemispheres of the Platesome-DiR group to the Liposome-Dir group. (**h**) Ex vivo fluorescence images of other major organs, including lung, heart, liver, spleen, and kidney, from mice treated with Liposome-DiR or Platesome-DiR for 24 h. (**i**) Fluorescence ratio of organs of the Platesome-DiR group to the Liposome-DiR group. n = 3, data are expressed as mean ± SEM. *$p < 0.05$.

kidney were imaged using an ex vivo imaging system. As shown in Figure 3f and g, the fluorescence signals in the injured brain from mice administered with Platesome-DiR were greater than those in the Liposome-DiR group, indicating that Platesome-DFO possesses enhanced stroke lesion targetability. The fluorescence signals in the other major organs of Liposome-DiR mice and Platesome-DiR mice were similar; the fluorescence signals visibly accumulate in the liver (Figure 3h and i), which is consistent with previously reported nanoparticles of similar size.[14] In brief, our results confirm that Platesome-DFO can target the injured brain in cerebral I/R.

https://doi.org/10.2147/IJN.S516316

Platesome-DFO Alleviates Cerebral I/R-Induced Brain Damage in Mice

To evaluate whether Platesome-DFO can provide therapeutic benefits to the ischemic brain, we established I/R model in mice and assessed the degree of brain damage after treatment of nanoparticles. As shown in Figure 4a and b, the encapsulation and loading efficiencies of DFO in Platesome-DFO were 9.54 ± 1.18% and 27.78 ± 2.47%, respectively. First, we evaluated the cell uptake and antioxidative function of Platesome-DFO in vitro. DiO (3,3′-Dioctadecyloxacarbocyanine Perchlorate)-encapsulated liposomes (Liposome-DiO) and platesomes (Platesome-DiO) were prepared and incubated with Neuro-2a (N2a) cells alongside free DiO. Both Liposome-DiO and Platesome-DiO significantly enhanced cellular uptake compared to free DiO, with Platesome-DiO achieving the highest intracellular accumulation (Figure 4c and d).

To evaluate the antioxidant efficacy of Platesome-DFO, an in vitro I/R model was established in N2a cells by exposing them to oxygen-glucose deprivation and reoxygenation (OGD/R). Free DFO, Liposome-DFO, or Platesome-DFO was administered during the reoxygenation phase. Results demonstrated that both Liposome-DFO and Platesome-DFO significantly attenuated OGD/R-induced ROS generation, and Platesome-DFO group exhibited the lowest ROS levels among all groups, highlighting its superior antioxidant capacity against OGD/R injury (Figure 4e and f). Subsequently, we evaluated the therapeutic effects of Platesome-DFO on I/R injury in vivo. After 1 h of MCAO, we intravenously injected saline, DFO, Liposome-DFO, PNV, or Platesome-DFO (25 mg/kg equiv. DFO) at the beginning of reperfusion. Neurological deficit assessment revealed that MCAO mice receiving Platesome-DFO treatment showed markedly lower scores, indicating decreased brain damage compared to the other groups (Figure 4g). Furthermore, we evaluated the infraction volumes in the stroke brain by TTC staining. The Platesome-DFO-treated stroke mice exhibited a significantly smaller ischemic area than in the other groups, including saline, free DFO, Liposome-DFO and PNV groups (Figure 4h and i). The inflammatory response is a major culprit in I/R-induced neuronal death and can be used to evaluate the degree of I/R damage.[32] Therefore, we proceeded to examine the mRNA expression of major pro-inflammatory cytokines in the penumbra of mice in the different groups. The levels of interleukin 6 (IL6), interleukin 1β (IL1β), and tumor necrosis factor α (TNFα) on the I/R side of the brain were significantly increased, with the level in Platesome-DFO treated group markedly lower than that in the other groups (Figure 4j–L). Taken together, our data indicate that Platesome-DFO injection can alleviate I/R-induced brain damage, supporting this nanoformulation as a candidate medicine for ischemic stroke therapy.

Platesome-DFO Effectively Removes Excessive Iron in Stroke Lesions and Inhibits Neuronal Ferroptosis

Iron overload and iron-dependent lipid ROS generation play a central role in I/R-induced ferroptosis, so inhibiting brain iron accumulation is a means to prevent neuronal cell death during stroke treatment. We therefore addressed whether Platesome-DFO can inhibit iron overload in stroke mice. Inductively coupled plasma-mass spectrometry (ICP-MS) analysis revealed that the iron content was increased in the injured region of the I/R brain compared to the control side. As expected, Platesome-DFO treatment significantly attenuated the I/R-induced iron accumulation (Figure 5a); the iron levels in the I/R side of the brain in Platesome-DFO treated mice was almost completely reversed to the levels of the control side. Next, we assessed the expression of FtH and FtL, the heavy chain and light chain subunits of the cytosolic iron storage protein, ferritin, which is an indicator of cellular iron status. As shown in Figure 5b-d, the levels of FtH and FtL were markedly increased in the penumbra of the I/R brain, with the increase significantly reduced in mice receiving Platesome-DFO treatment, indicating that Platesome-DFO alleviated the I/R-associated iron overload. Ferroptosis, a recently defined cell death caused by iron-dependent lipid ROS accumulation, plays a key role in the pathogenesis of ischemic stroke. Therefore, we examined the effects of Platesome-DFO on I/R-induced ferroptosis. The mRNA expression of prostaglandin-endoperoxide synthase 2 gene (*Ptgs2*), a biomarker of ferroptosis, was markedly increased on the I/R side of the brain in the saline, DFO, Liposome-DFO, and PNV groups, while treatment with Platesome-DFO inhibited the up-regulation of *Ptgs2* (Figure 5e). The expression of ACSL4 (acyl-CoA synthetase long-chain family member 4), a positive regulator of ferroptosis which catalyzes the formation of lipid ROS, was increased in the penumbra in the saline, DFO, Liposome-DFO, and PNV groups, while, again, Platesome-DFO treatment led to a significantly

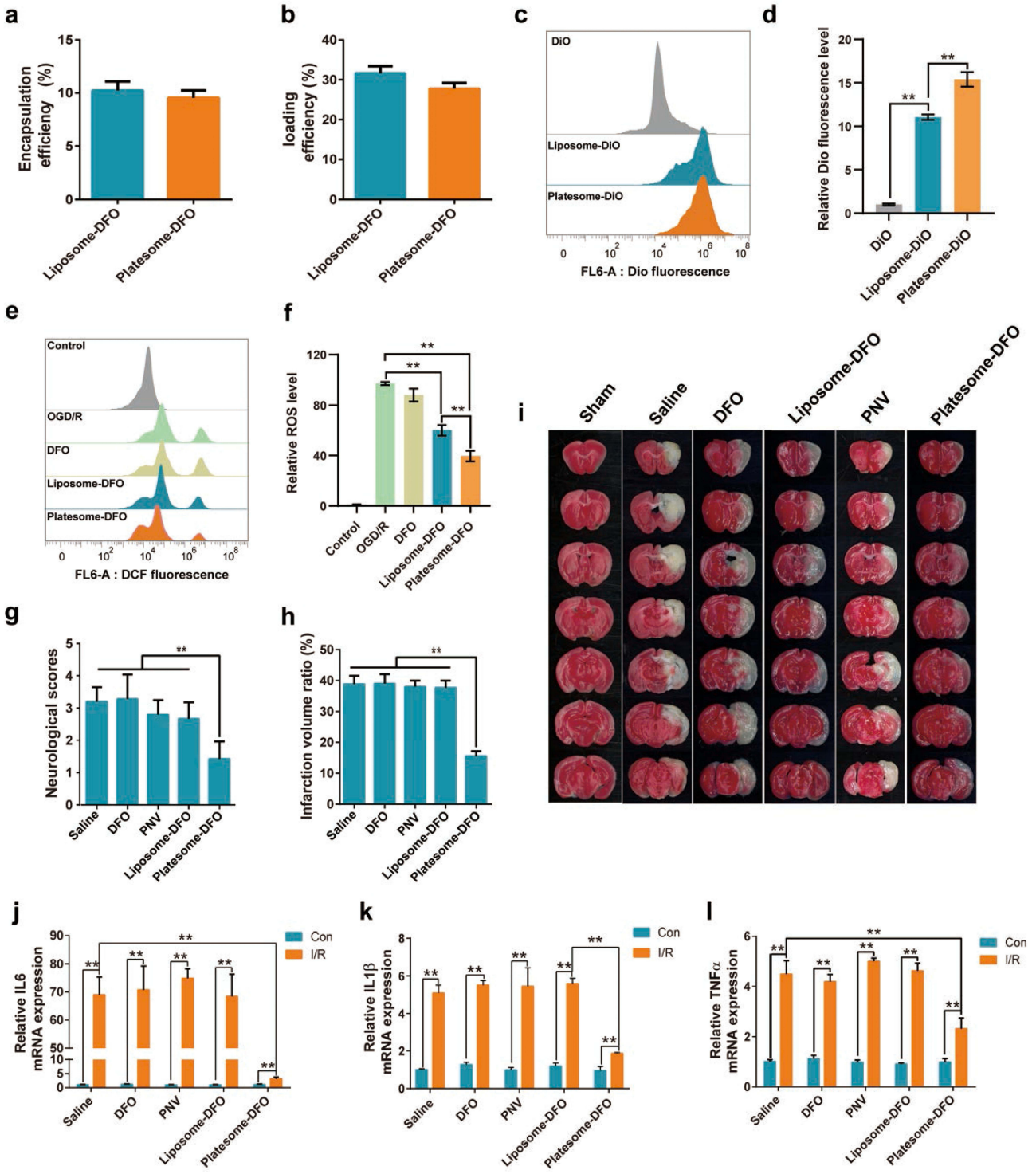

Figure 4 Platesome-DFO alleviates cerebral I/R-induced brain damage in mice. (**a**) Encapsulation and (**b**) loading efficiencies of DFO in Liposome-DFO and Platesome-DFO were measured spectrophotometrically. (**c**) Flow cytometry analysis of cellular DiO levels in N2a cells treated with free DiO, Liposome-DiO, or Platesome-DiO. (**d**) Cellular DiO fluorescence level analysis (n=3). (**e**) Flow cytometry was performed to quantify OGD/R-induced ROS generation (measured by DCF fluorescence) in N2a cells treated with free DFO, Liposome-DFO, or Platesome-DFO during the reoxygenation phase. (**f**) ROS content analysis (n=3). (**g**) Neurological scores of stroke mice after treatment with saline, DFO, Liposome-DFO, PNV, or Platesome-DFO, (n=15). The infarct region appears as white, while the normal region is red. (**h**) Quantification of brain infarction volume ratio at 24 h after saline, DFO, Liposome-DFO, PNV, or Platesome-DFO treatment, (n = 5). (**i**) Representative TTC-stained brain sections from stroke model mice from the indicated groups. (**j-l**) Relative mRNA levels of (**j**) IL6, (**k**) IL1β, and (**l**) TNFα, were measured in the contralateral (Con) and I/R sides of the brain in the indicated groups (n = 4). The mRNA levels were normalized to β-actin mRNA levels and are shown relative to the mean value in the Con side of the saline-treated stroke mice. I/R, penumbral area in the cortex of the injured hemisphere; Con, the same area in the penumbra in the cortex of the contralateral hemisphere. Data are expressed as mean ± SEM. $^{**}p < 0.01$.

https://doi.org/10.2147/IJN.S516316

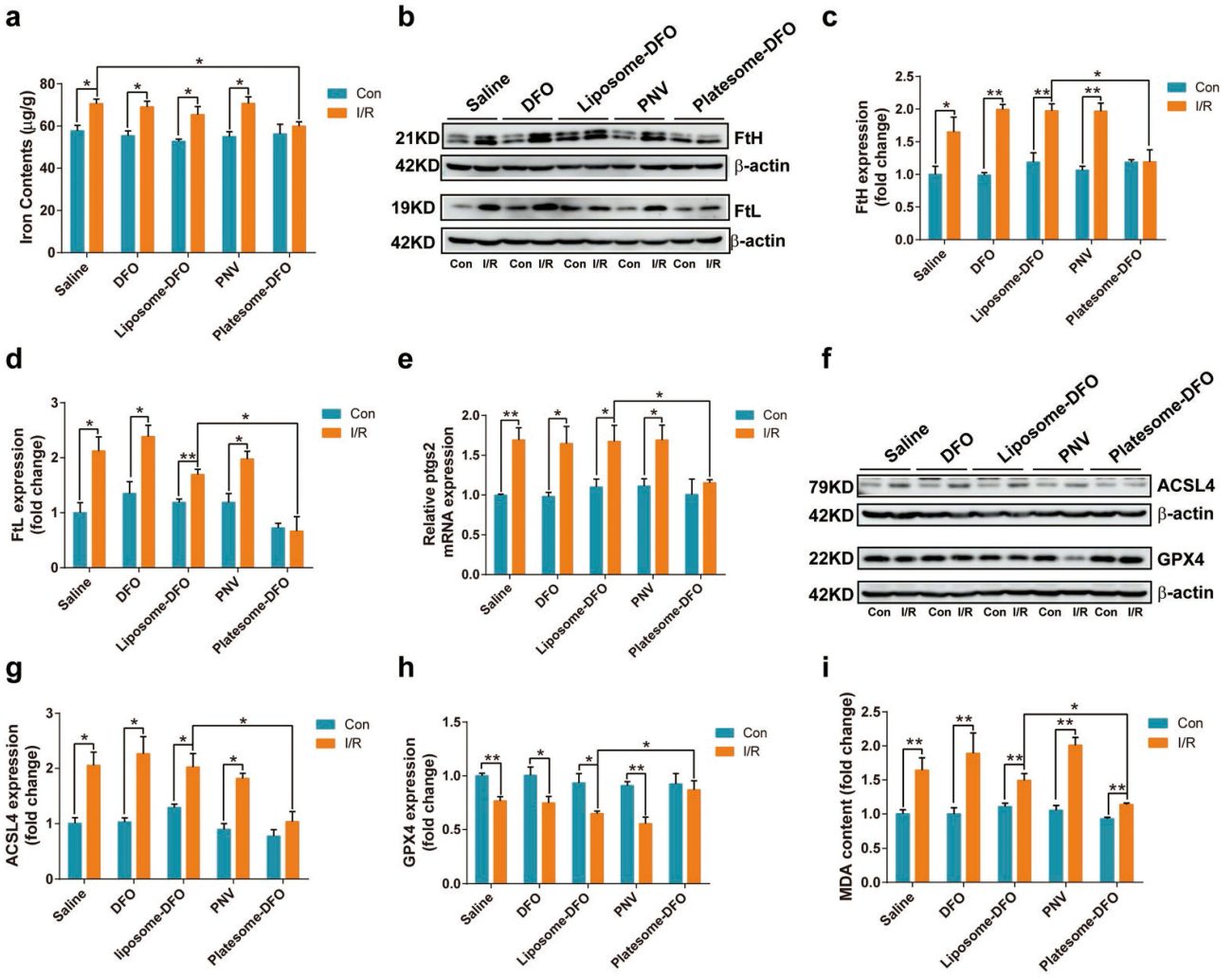

Figure 5 Platesome-DFO effectively removes excessive iron in stroke lesions and inhibits neuronal ferroptosis. (**a**) Assessment of iron contents by ICP-MS in the indicated groups (n = 5). (**b**) Western blot analysis of the iron storage proteins FtH and FtL (n = 4). (**c** and **d**) Quantification of (**c**) FtH and (**d**) FtL expression in the indicated groups. (**e**) Relative mRNA level of *Ptgs2* in the contralateral (Con) and I/R sides of the brain in the indicated groups. The mRNA levels were normalized to β-actin mRNA levels and are shown relative to the mean value in the Con side of saline-treated stroke mice (n = 4). (**f**) Western blot analysis of the ferroptosis-associated proteins, Acsl4 and GPX4 (n = 4). (**g** and **h**) Quantification of (**g**) ACSL4 and (**h**) GPX4 expression in the indicated groups. (**i**) MDA contents in saline group, DFO group, Liposome-DFO group, PNV group, and Platesome-DFO group brains. The results are expressed relative to the mean value in the Con side of saline group (n = 5). Data are expressed as mean ± SEM. $^{*}p < 0.05$ $^{**}p < 0.01$.

decrease (Figure 5f and g). Meanwhile, the level of the negative regulator of ROS, glutathione peroxidase 4 (GPX4), was higher in the stroke mice receiving Platesome-DFO than the other groups (Figure 5f and h). Platesome-DFO injection attenuated the blockade of the antioxidant protein and, as a result, alleviated I/R-induced ferroptosis. The biochemical mechanism underlying ferroptosis is the production of lipid-associated ROS to a lethal dose. We measured MDA (malondialdehyde) content to assess lipid peroxidation and found that the production of MDA on the I/R side of the brain was significantly increased in all MCAO mice, compared to the control side. However, the Platesome-DFO I/R group had significantly lower levels than the other groups (Figure 5i). These results provide molecular evidence that Platesome-DFO treatment effectively removed excessive iron in stroke lesion and inhibited neuronal ferroptosis.

Biosafety Evaluation of Platesome-DFO

Finally, we investigated the safety of Platesome-DFO. H&E (hematoxylin-eosin) staining did not reveal any apparent abnormalities or pathological changes in the major organs, including brain, heart, liver, spleen, lung, and kidney, derived from mice administered Platesome-DFO (Figure 6a and b). Nor were there any changes in their serum biochemical indicators of liver or kidney function (Figure 6c-f). The results from hemolysis experiments suggest that none of the nanoparticles induced marked

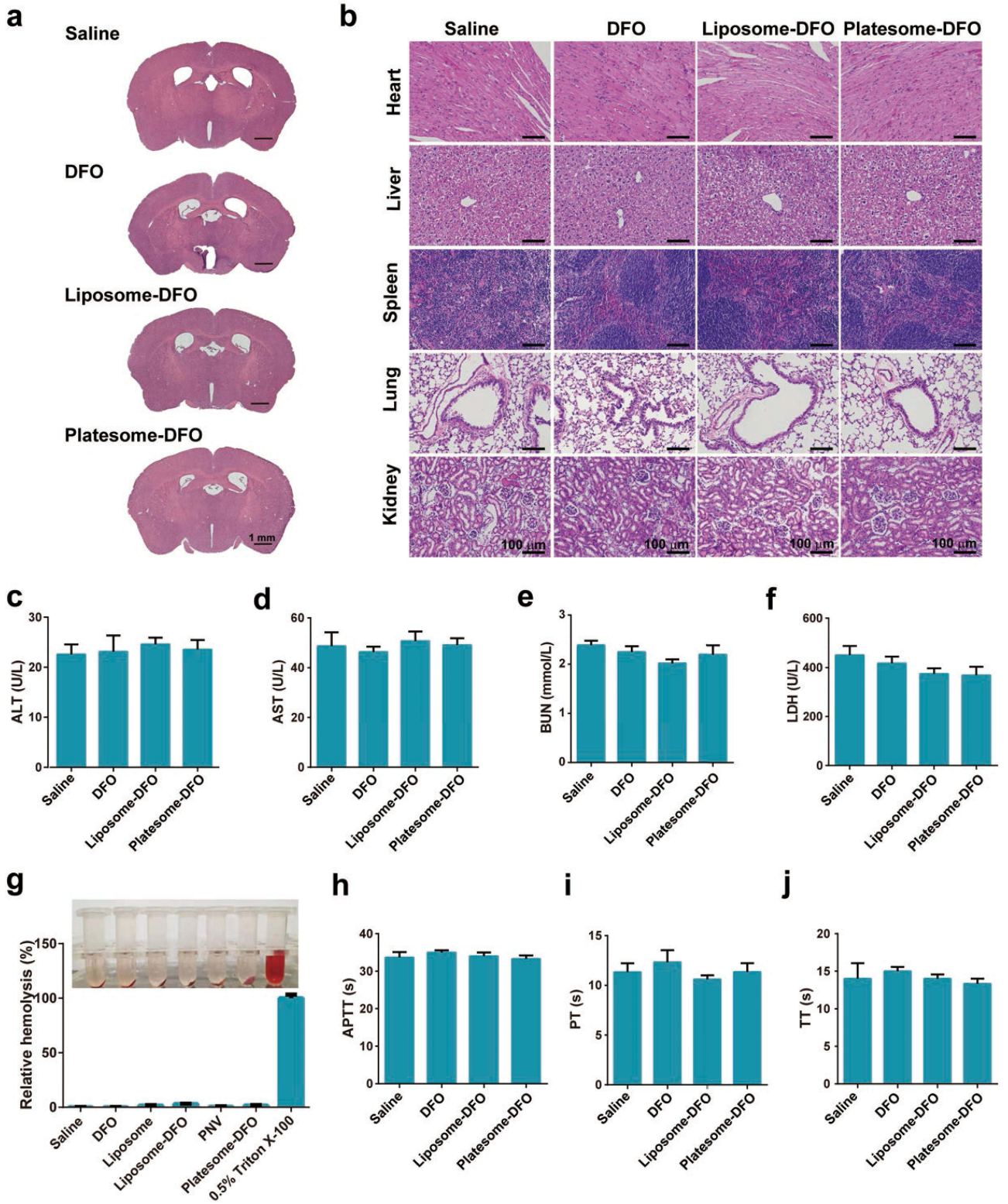

Figure 6 Biosafety evaluation of Platesome-DFO. Representative images of histopathology of the brain (**a**), heart, liver, spleen, lung, and kidney (**b**) resected from mice following saline, DFO, Liposome-DFO, PNV, or Platesome-DFO administration. (**c**–**f**) Serum biochemical analysis of mice treated with the indicated nanoparticles. (**c**) Alanine transaminase (ALT); (**d**) aspartate transaminase (AST); (**e**) blood urea nitrogen (BUN); (**f**) lactate dehydrogenase (LDH). (**g**) The hemolytic potential of the nanoparticles, including saline, DFO, Liposome-DFO, PNV, and Platesome-DFO, and a positive control (0.5% Triton X-100 in saline). Data are expressed relative to the Triton X-100 control group. (**h**–**j**) Coagulation indices, including (**h**) APTT, (**i**) PT, and (**j**) TT were measured in mice treated with the indicated drug formulations. Data are expressed as mean ± SEM., n = 3.

https://doi.org/10.2147/IJN.S516316

hemolysis (>5%) when incubated with red blood cells, while the positive control, Triton X-100 treatment, caused significant hemolysis (Figure 6g). To verify whether Platesome-DFO treatment activates the coagulation system in mice, we also examined coagulation-related indicators, including activated partial thromboplastin time (APTT), prothrombin time (PT), and thrombin time (TT), in the plasma from mice after Platesome-DFO treatment. No detectable differences were observed in any of the measured indicators between the Platesome-DFO group and the saline group (Figure 6h-j). These results indicate that Platesome-DFO can efficiently reduce brain iron content, inhibit ferroptotic cell death, and alleviate I/R-induced brain injury without apparent side effects, further supporting Platesome-DFO as a potential medicine for treating ischemic stroke.

Discussion

As a transition metal, iron in the brain plays a crucial role in maintaining physiological functions by participating in many essential cellular activities, such as mitochondrial respiration and neurotransmitter synthesis.[33] However, excessive brain iron is a potent source of oxidative damage through catalyzing hydroxyl radical production via the Fenton reaction and the Haber-Weiss cycle, leading to ROS accumulation in neuronal cells. In addition, several lipid oxidation enzymes, such as LOX, are iron-containing or iron-dependent enzymes that can facilitate lethal lipid-ROS generation. Previous clinical and experimental research has demonstrated that ischemic stroke causes disruption of brain iron metabolism, thus leading to iron accumulation in the stroke lesion. Our recent series of studies further confirmed that inhibiting iron overload by regulating iron-related proteins, such as endothelial ferroportin 1 and mitochondrial ferritin, significantly alleviates cerebral I/R-induced neuronal damage, indicating that iron is a potential target for ischemic stroke treatment.[8,34] In this study, we chose DFO, an FDA-approved iron chelator, as the therapeutic drug and designed a platelet membrane-coated liposome delivery platform to overcome the drawbacks of DFO in clinical applications, including poor bioavailability, short plasma half-life, and liver toxicity. The exceptional therapeutic advantages of Platesome-DFO that we observed, ranging from high iron chelation efficiency and inhibition of ferroptosis to significant improvement in neurological deficits, highlight that this nanoformulation is a promising treatment approach for cerebral I/R injury and that iron homeostasis represents a potential therapeutic target for developing novel drugs for ischemic stroke. In addition, although previous studies on I/R injury therapy primarily focused on scavenging pre-existing ROS in stroke lesions, the persistent ROS generation following I/R injury is frequently neglected, which may lead to suboptimal therapeutic outcomes. In contrast, our study presents a novel strategy by modulating iron homeostasis in stroke lesions via Platesome-DFO, which simultaneously inhibits ROS production and suppresses ferroptosis signaling, offering enhanced therapeutic potential against I/R-induced damage.

Nano-based drug delivery systems are spawning a paradigm shift in the treatment of refractory human diseases because nanomaterials have high design flexibility and can significantly improve pharmacokinetics and reduce side effects of the delivered drugs.[22,23,35] The blood–brain barrier (BBB) is essential for the brain to maintain the ionic homeostasis within the CNS. However, disruption of BBB integrity has been well documented following ischemic stroke and has been reported to further exacerbate I/R-induced brain injury. Our previous study has demonstrated that nano-liposomes possess advantages in carrying hydrophilic substances and crossing the leaky BBB in ischemic stroke.[27] Therefore, we first encapsulated DFO within liposomes to improve its biocompatibility and assist the nanoparticles in crossing the leaky BBB. High concentration of DFO in stroke lesion is pivotal in improving stroke outcomes and reducing side effects associated with systemic DFO administration. Given the inherent properties of platelets in binding to injured vasculature and the development of platelet biomimetic nanoparticles, we further coated PLT membrane onto the DFO liposome to increase the concentration of Platesome-DFO in the stroke brain. As shown in Figure 3, Platesome-DFO exhibited the highest concentration in the stroke lesion. Particularly, Platesome-DFO application is safe and effective in preventing brain injury following stroke, with no apparent side effects (Figure 6). Significantly, the majority of components in the Platesome-DFO formulation, including the iron chelator DFO and liposomal carrier, are FDA-approved pharmaceutical agents, which may substantially lower regulatory barriers for clinical translation of this therapeutic platform. However, despite the multiple therapeutic advantages of platelet membrane coating technology in I/R injury management, our current utilization of allogeneic platelet sources may raise potential concerns regarding immunogenicity in clinical applications. Therefore, the systematic evaluation of immunoreactive risks and the development of in vitro-generated platelet alternatives remain imperative for future studies.

Several cell death pathways, including apoptosis, necroptosis, and ferroptosis, have been reported to contribute to neurological damage in ischemic stroke, especially in I/R injury. As a co-factor involved in ROS generation, iron is believed

to participate in many cell death pathways. However, recent studies highlight that iron plays a key role in I/R-induced ferroptosis, an iron-dependent cell death.[8,10,36] Therefore, we primarily tested the effects of Platesome-DFO on ferroptosis pathways, and we hope to further evaluate the detailed impacts of this nanoparticle on other pathways in future studies.

Conclusion

In summary, here we have reported a platelet membrane-cloaked liposome nanocarrier to deliver the iron chelator, DFO, to stroke lesions for the treatment of cerebral I/R injury. The platelet membrane plays important roles in targeting the injured brain in ischemic stroke. The platelet components in the Platesome-DFO nanoparticle retained the natural advantages of platelet, that gives Platesome-DFO the ability to target stroke lesion efficiently. After intravenous administration to stroke model mice, the Platesome-DFO efficiently sequestered toxic iron, inhibiting the activation of ferroptosis, ultimately attenuating cerebral I/R-induced neuronal cell death and neurological deficits. No detectable side effects in the major organs were observed after treatment with Platesome-DFO. Taken together, the Platesome-DFO we formulated presents a potential treatment strategy for cerebral ischemia reperfusion injury.

Data Sharing Statement

Data will be made available on request from the corresponding author.

Acknowledgments

The work was supported by the National Natural Science Foundation of China (32300797, U23A20169), the Key Project of Natural Science Foundation of Hebei Province, China (E2021205003), Hebei Natural Science Foundation (C2022206006) and the Science and Technology Research Project of Universities in Hebei Province, China (BJK2024181).

Author Contributions

All authors made a significant contribution to the work reported, whether that is in the conception, study design, execution, acquisition of data, analysis and interpretation, or in all these areas; took part in drafting, revising or critically reviewing the article; gave final approval of the version to be published; have agreed on the journal to which the article has been submitted; and agree to be accountable for all aspects of the work.

Disclosure

The authors declare that they have no known competing financial interests or personal relationships that could have appeared to influence the work reported in this paper.

References

1. Cui P, Hou H, Song B, Xia Z, Xu Y. Vitamin D and ischemic stroke - Association, mechanisms, and therapeutics. *Ageing Res Rev*. 2024;96:102244. doi:10.1016/j.arr
2. Li X, Han Z, Wang T, et al. Cerium oxide nanoparticles with antioxidative neurorestoration for ischemic stroke. *Biomaterials*. 2022;291:121904. doi:10.1016/j.biomaterials
3. Dávalos A, Castillo J, Marrugat J, et al. Body iron stores and early neurologic deterioration in acute cerebral infarction. *Neurology*. 2000;54:1568–1574. doi:10.1212/wnl.54.8.1568
4. Millan M, Sobrino T, Castellanos M, et al. Increased body iron stores are associated with poor outcome after thrombolytic treatment in acute stroke. *Stroke*. 2007;38:90–95. doi:10.1161/01.STR.0000251798.25803.e0
5. Millán M, Degregorio-Rocasolano N, Np DLO, et al. Article targeting pro-oxidant iron with deferoxamine as a treatment for ischemic stroke: safety and optimal dose selection in a randomized clinical trial. *Antioxidants*. 2021;10(8):1270. doi:10.3390/antiox10081270
6. He Q, Wang W, Xu D, et al. Causal association of iron status with functional outcome after ischemic stroke. *Stroke*. 2024;55:423–431. doi:10.1161/STROKEAHA.123.044930
7. Wang P, Ren Q, Shi M, Liu Y, Bai H, Chang YZ. Overexpression of mitochondrial ferritin enhances blood–brain barrier integrity following ischemic stroke in mice by maintaining iron homeostasis in endothelial cells. *Antioxidants*. 2022;11(7):1257. doi:10.3390/antiox11071257
8. Wang P, Cui Y, Ren Q, et al. Mitochondrial ferritin attenuates cerebral ischaemia / reperfusion injury by inhibiting ferroptosis. *Cell Death Dis*. 2021;12(5):447. doi:10.1038/s41419-021-03725-5
9. Ding H, Cz Y, Shi H, et al. Hepcidin is involved in iron regulation in the ischemic brain. *PLoS One*. 2011;6:1–10. doi:10.1371/journal.pone.0025324

10. Qz T, Lei P, Ka J, et al. Tau-mediated iron export prevents ferroptotic damage after ischemic stroke. *Mol Psychiatry*. 2017;22:1520–1530. doi:10.1038/mp.2017.171
11. Sj D, Km L, Mr L, et al. Ferroptosis: an iron-dependent form of nonapoptotic cell death. *Cell*. 2012;149:1060–1072. doi:10.1016/j.cell.2012.03.042
12. zhang TQ, Liu Y, Xiang Z, et al. Thrombin induces ACSL4-dependent ferroptosis during cerebral ischemia/reperfusion. *Signal Transduct Target Ther*. 2022;7:7. doi:10.1038/s41392-022-00917-z
13. Bayanzay K, Alzoebie L. Reducing the iron burden and improving survival in transfusion-dependent thalassemia patients: current perspectives. *J Blood Med*. 2016;7:159–169. doi:10.2147/JBM.S61540
14. You L, Wang J, Liu T, et al. Targeted brain delivery of rabies virus glycoprotein 29-modified deferoxamine-loaded nanoparticles reverses functional deficits in parkinsonian mice. *ACS Nano*. 2018;12:4123–4139. doi:10.1021/acsnano.7b08172
15. Ds I, Jw J, Js L, et al. Role of the NMDA receptor and iron on free radical production and brain damage following transient middle cerebral artery occlusion. *Brain Res*. 2012;1455:114–123. doi:10.1016/j.brainres.2012.03.025
16. Abdul Y, Li W, Ward R, et al. Deferoxamine treatment prevents post-stroke vasoregression and neurovascular unit remodeling leading to improved functional outcomes in type 2 male diabetic rats: role of endothelial ferroptosis. *Transl Stroke Res*. 2021;12:615–630. doi:10.1007/s12975-020-00844-7
17. Selim M. Treatment with the iron chelator, deferoxamine mesylate, alters serum markers of oxidative stress in stroke patients. *Transl Stroke Res*. 2010;1:35–39. doi:10.1007/s12975-009-0001-0
18. Lang J, Zhao X, Wang X, et al. Targeted co-delivery of the iron chelator deferoxamine and a HIF1α inhibitor impairs pancreatic tumor growth. *ACS Nano*. 2019;13:2176–2189. doi:10.1021/acsnano.8b08823
19. Kosyakovsky J, Fine JM, Frey WH, Hanson LR. Mechanisms of intranasal deferoxamine in neurodegenerative and neurovascular disease. *Pharmaceuticals*. 2021;14:1–14. doi:10.3390/ph14020095
20. Li C, Sun T, Jiang C. Recent advances in nanomedicines for the treatment of ischemic stroke. *Acta Pharm Sin B*. 2021;11:1767–1788. doi:10.1016/j.apsb.2020.11.019
21. Wang R, Nie W, Yan X, et al. Biomimetic nanomotors for deep ischemia penetration and ferroptosis inhibition in neuroprotective therapy of ischemic stroke. *Adv Mater*. 2025;37(3):e2409176. doi:10.1002/adma.202409176
22. Li M, Liu Y, Chen J, et al. Platelet bio-nanobubbles as microvascular recanalization nanoformulation for acute ischemic stroke lesion theranostics. *Theranostics*. 2018;8:4870–4883. doi:10.7150/thno.27466
23. Xu J, Zhang Y, Xu J, et al. Engineered nanoplatelets for targeted delivery of plasminogen activators to reverse thrombus in multiple mouse thrombosis models. *Adv Mater*. 2020;32:1–14. doi:10.1002/adma.201905145
24. Li M, Li J, Chen J, et al. Platelet membrane biomimetic magnetic nanocarriers for targeted delivery and in situ generation of nitric oxide in early ischemic stroke. *ACS Nano*. 2020;14:2024–2035. doi:10.1021/acsnano.9b08587
25. Li Y, Teng X, Yang C, et al. Ultrasound controlled anti-inflammatory polarization of platelet decorated microglia for targeted ischemic stroke therapy. *Angewandte Chemie - Int Ed*. 2021;60:5083–5090. doi:10.1002/anie.202010391
26. Xu J, Wang X, Yin H, et al. Sequentially site-specific delivery of thrombolytics and neuroprotectant for enhanced treatment of ischemic stroke. *ACS Nano*. 2019;13:8577–8588. doi:10.1021/acsnano.9b01798
27. Zhao Y, Xin Z, Li N, et al. *Nano-liposomes of Lycopene Reduces Ischemic Brain Damage in Rodents by Regulating Iron Metabolism*. Elsevier B.V; 2018. doi:10.1016/j.freeradbiomed
28. Liu G, Zhao X, Zhang Y, et al. Engineering biomimetic platesomes for ph-responsive drug delivery and enhanced antitumor activity. *Adv Mater*. 2019;31:1–12. doi:10.1002/adma.201900795
29. Wang P, Wu Q, Wu W, et al. Mitochondrial ferritin deletion exacerbates β -amyloid-induced neurotoxicity in mice. *Oxid Med Cell Longev*. 2017;2017:1–24. doi:10.1155/2017/1020357
30. Jin M, Jh K, Jang E, et al. Lipocalin-2 deficiency attenuates neuroinflammation and brain injury after transient middle cerebral artery occlusion in mice. *J Cereb Blood Flow Metab*. 2014;34:1306–1314. doi:10.1038/jcbfm.2014.83
31. Wang S, Duan Y, Zhang Q, et al. Drug targeting via platelet membrane–coated nanoparticles. *Small Struct*. 2020;1:2000018. doi:10.1002/sstr.202000018
32. Anrather J, Iadecola C. Inflammation and Stroke: an Overview. *Neurotherapeutics*. 2016;13:661–670. doi:10.1007/s13311-016-0483-x
33. Wang Z, Yn Z, Yang P, et al. Axonal iron transport in the brain modulates anxiety-related behaviors. *Nat Chem Biol*. 2019;15:1214–1222. doi:10.1038/s41589-019-0371-x
34. Zheng H, Guo X, Kang S, et al. Cdh5-mediated Fpn1 deletion exerts neuroprotective effects during the acute phase and inhibitory effects during the recovery phase of ischemic stroke. *Cell Death Dis*. 2023;14:14. doi:10.1038/s41419-023-05688-1
35. Yu W, Yin N, Yang Y, et al. Rescuing ischemic stroke by biomimetic nanovesicles through accelerated thrombolysis and sequential ischemia-reperfusion protection. *Acta Biomater*. 2022;140:625–640. doi:10.1016/j.actbio.2021.12.009
36. Du B, Deng Z, Chen K, et al. Iron promotes both ferroptosis and necroptosis in the early stage of reperfusion in ischemic stroke. *Genes Dis*. 2024;11:11. doi:10.1016/j.gendis.2024.101262